ARL-TR-8335 • Mar 2018

US Army Research Laboratory

Influence of Test Section Geometry on the Blast Environment in an Explosively Driven Conical Shock Tube

by Joel B Stewart

NOTICES

Disclaimers

The findings in this report are not to be construed as an official Department of the Army position unless so designated by other authorized documents.

Citation of manufacturer's or trade names does not constitute an official endorsement or approval of the use thereof.

Destroy this report when it is no longer needed. Do not return it to the originator.

ARL-TR-8335 ● MAR 2018

US Army Research Laboratory

Influence of Test Section Geometry on the Blast Environment in an Explosively Driven Conical Shock Tube

by Joel B Stewart
Weapons and Materials Research Directorate, ARL

REPORT DOCUMENTATION PAGE

Form Approved
OMB No. 0704-0188

PLEASE DO NOT RETURN YOUR FORM TO THE ABOVE ADDRESS.

1. REPORT DATE *(DD-MM-YYYY)*	2. REPORT TYPE	3. DATES COVERED (From - To)
March 2018	Technical Report	January 2017–July 2017

4. TITLE AND SUBTITLE
Influence of Test Section Geometry on the Blast Environment in an Explosively Driven Conical Shock Tube

5a. CONTRACT NUMBER

5b. GRANT NUMBER

5c. PROGRAM ELEMENT NUMBER

6. AUTHOR(S)
Joel B Stewart

5d. PROJECT NUMBER
AH80

5e. TASK NUMBER

5f. WORK UNIT NUMBER

7. PERFORMING ORGANIZATION NAME(S) AND ADDRESS(ES)
US Army Research Laboratory
ATTN: RDRL-WMP-G
Aberdeen Proving Ground, MD 21005

8. PERFORMING ORGANIZATION REPORT NUMBER
ARL-TR-8335

9. SPONSORING/MONITORING AGENCY NAME(S) AND ADDRESS(ES)

10. SPONSOR/MONITOR'S ACRONYM(S)

11. SPONSOR/MONITOR'S REPORT NUMBER(S)

12. DISTRIBUTION/AVAILABILITY STATEMENT
Approved for public release; distribution is unlimited.

13. SUPPLEMENTARY NOTES
primary author's email: <joel.b.stewart2.civ@mail.mil>.

14. ABSTRACT
This report details experimental data gathered on incident overpressures and the corresponding impulses obtained in the test section of an explosively driven 10° (full angle) conical shock tube. Due to the shock tube's steel walls approximating the boundary conditions seen by a spherical sector cut out of a detonating sphere of energetic material, a 5.3-g pentolite shock tube driver charge produces peak overpressures corresponding to a free-field detonation from an 816-g sphere of pentolite. The 4 test section geometries investigated in this report (open air, cylindrical, 10° inscribed square frustum, and 10° circumscribed square frustum) provide a variety of different time histories for the incident overpressures and impulses, with a circumscribed square frustum yielding the best approximation of the mid-field blast environment produced by a free-field detonation.

15. SUBJECT TERMS
air blast, shock tube, air shock, mid-field blast environment, explosively driven shock tube

16. SECURITY CLASSIFICATION OF:			17. LIMITATION OF ABSTRACT	18. NUMBER OF PAGES	19a. NAME OF RESPONSIBLE PERSON
a. REPORT	b. ABSTRACT	c. THIS PAGE			Joel B Stewart
Unclassified	Unclassified	Unclassified	UU	34	19b. TELEPHONE NUMBER (Include area code) 410-278-3129

Standard Form 298 (Rev. 8/98)
Prescribed by ANSI Std. Z39.18

Contents

List of Figures

List of Tables

Acknowledgments

Collin Pecora assisted with the design of the shock tube stand and gave technical advice throughout this project. Robert Spink was of great assistance in creating the engineering drawings for the planar test sections. Scott Kukuck and Barrie Homan were solicited for numerous technical reviews and discussions on explosively driven conical shock tubes, and their advice on the topic is greatly appreciated. Kevin McNesby reviewed an earlier draft of this report and his comments greatly improved the overall presentation. Brian Roos and Dawnn Megonnell were responsible for the coordination and fabrication of the shock tube explosive charges. Paul Duvall acted as the test director for the shock tube experimental program, and the author thanks him for his attention to detail and ensuring that the experimental series ran smoothly. Larry Stevenson, James Racine, and Jason Pierce were instrumental in setting up the diagnostic equipment in the experiments and collecting the data accurately and efficiently. The author is grateful to the US Army Research Laboratory shops for their fabrication assistance—specifically, to Bobby Hall and James Gyolai for milling the shock tube driver sections, to David Weyand for press-braking the pieces comprising the channel section and welding the test sections, and to Gerard Chaney for constructing the wooden stand and fabricating the foam centering devices.

INTENTIONALLY LEFT BLANK.

1. Introduction

The study of shock waves being propagated through tubes has been ongoing for more than 2 centuries.[1–3] These devices are denoted as shock tubes and they provide a controlled environment for investigating shock waves traveling through various media as well as the interaction of these disturbances with other structures. When used to study the environment from detonating energetic material, shock tubes have an advantage over free-field experiments in that the shock tube walls confine and focus the detonation event, limiting the hazardous region and resulting in the potential to use more sophisticated and expensive equipment than would otherwise be practical.

An explosive air blast environment can be categorized into 3 regions:[4,5]

- The near-field region covers the extent of detonation product expansion. The incident overpressures in this region are generally greater than 1 MPa.
- The mid-field is the region beyond the fireball where non-uniform effects such as late-time combustion or non-spherical charge shape still contribute significantly to the flow field. The incident overpressures in this region tend to range from 100 kPa to 1 MPa, with the positive phase often described using a modified Friedlander equation.[6] This description of the waveform adds a shape factor to the original Friedlander equation[7] that varies with explosive material and distance from the charge.
- The far-field is the region where non-uniform effects are largely absent. In this region, the incident overpressures are typically less than 100 kPa and the positive phase loading profile can be approximated using the original Friedlander equation.[6]

When shock tubes are used to conduct blast research, the goal is to simulate the environment experienced in at least 1 of the 3 previously listed regions.

Shock tubes generally fall into 1 of 3 categories: 1) compression-driven tubes, where a shock wave is generated when high-pressure gases burst a frangible diaphragm; 2) combustion-driven devices, where combustible gases are ignited to

A condensed version of this report was published in the journal *Shock Waves*.[8]

generate a shock wave; and 3) explosively driven shock tubes, where a detonating energetic material generates the shock wave. There are challenges associated with operating any type of shock tube and accurately producing the particular waveforms of interest; the appropriate tool depends both on the application of interest and on the available facilities.

There is considerable literature on the development and use of compression-driven shock tubes,[9–12] which are relatively straightforward to incorporate into indoor facilities. Additionally, there have been recent developments in combustion-driven shock tube designs,[5,13,14] which seek to avoid issues in compression-driven tubes associated with non-uniform diaphragm rupture and poor approximations of free-field waveforms. In contrast to the first 2 types of shock tubes, explosively driven designs are not as prevalent, especially outside of government laboratories, since they require specialized facilities and personnel for handling energetic material. However, explosively driven shock tubes have the advantage of being able to readily replicate the environments characteristic of detonative events, certain aspects of which can be challenging for either compression- or combustion-driven tubes. In particular, if the energetic material of interest is used as the shock tube driver charge, explosively driven shock tubes can be used to study all 3 regions of a blast environment since the detonation products are included in the shock tube environment. This inclusion of detonation products can be especially important when investigating the late-time energy release characteristic of non-ideal explosives, since these late-time reactions yield higher impulses than what one would expect from more traditional explosives.

A number of authors have demonstrated the ability to use explosively driven shock tubes with conical geometries to approximate the mid- to far-field blast environment due to explosive detonations using relatively smaller charges.[5,15–18] The use of small explosive masses in the shock tube to mimic larger free-field detonations is possible because the shock tube acts as a spherical sector being cut out of a spherical detonation, with the shock tube walls approximating the boundary conditions seen at the surface of the spherical sector. Stewart and Pecora[18] used an explosively driven 17° (full angle) conical shock tube to approximate the blast environment from a 680–907 g (1.5–2.0 lb) composition C4 free-field detonation using a 14.5-g C4 shock tube explosive charge. This earlier work demonstrated the need for alleviating release waves at the shock tube channel section exit where test items would generally be placed.

The current work analyzes the influence that the geometry of the shock tube test section (i.e., the region where test items are placed) has on the measured overpressures and impulses downstream of the detonating charge, with a focus on accurately replicating the positive phase duration in the mid-field blast environment resulting from a spherical detonation in air. The motivation to investigate different test section geometries stems from a desire to use optical diagnostics, such as the high-brightness imaging used in McNesby et al.,[19] to visualize the flow around objects of interest and is a logical progression to the demonstrated effect of release waves in Stewart and Pecora.[18] The use of these optical diagnostics necessitates either placing test items outside the shock tube in the open air or installing a window into the shock tube test section—ideally a planar window to avoid issues with beam refraction through curved surfaces.

2. Technical Approach

2.1 Parts of the Explosively Driven Shock Tube

The work presented in this report focuses on experimental data gathered using an explosively driven 10° (full angle) conical shock tube (see Fig. 1 for a schematic of a generic explosively driven conical shock tube). The shock tube is manufactured from mild steel throughout and consists of 1) the driver section, which is a 2-part sacrificial piece composed of the housing section confining the explosive charge and a transition section used to transmit the highest pressure gases downstream; 2) the channel section, which transmits the air shock and product gases; and 3) the test section, which is the area where measurements are taken and/or items are placed in the flow.

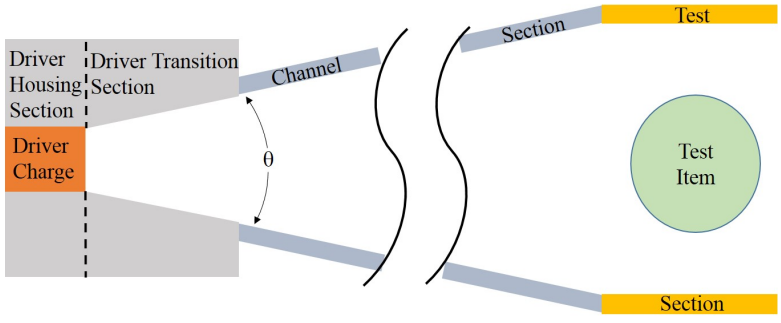

Fig. 1 Schematic of a generic explosively driven conical shock tube

The blast environment in the shock tube is quite dependent on the geometry of and the materials used in the driver housing section (see, for example, Stewart[20]). The mild steel driver section used for all experiments in this paper is the one shown in Fig. 2. The driver housing section consists of a 1.30-cm-long hollow right circular cylinder with a 6.35-cm outer diameter and a 1.78-cm inner diameter; the cylindrical explosive charge is also 1.30 cm long and 1.78 cm in diameter. The explosive material used for all data presented in the current work is 50/50 pentolite (i.e., 50% TNT and 50% PETN by mass). The charges were each nominally 5.3 g, resulting in an approximate density of 1.65 g/cm^3, and were all detonated using a Teledyne RISI RP-80 exploding bridgewire detonator (203 mg of explosive). The transition section is a 2.54-cm-long, 6.35-cm-outer-diameter cylinder with a 10° cone milled through the center, starting with the 1.78-cm inner diameter to mate up with the housing section.

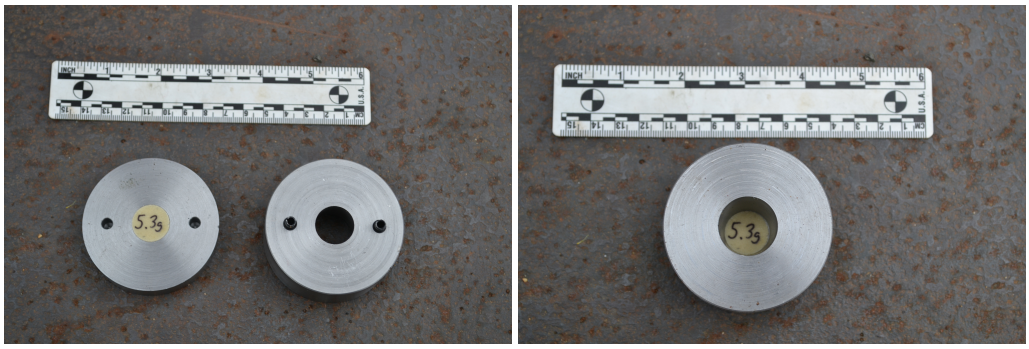

a) **b)**

Fig. 2 Pentolite explosive charge with the shock tube driver section: a) steel driver housing section with inserted 5.3-g pentolite charge (left) next to the steel driver transition section (right), and b) assembled driver section showing the downstream surface of the pentolite charge

The channel section of the shock tube used in this work consists of 7 30.5-cm-long 10° conical pieces that are each fabricated by press-braking 0.48-cm-thick (3/16 inches) mild steel sheets; typically, 2 halves are press-braked for each 30.5-cm piece, which are then welded together. The last piece of the channel section is approximately 40 cm in diameter at the largest end (i.e., the channel exit). The channel sections were made in 7 separate pieces to facilitate future plans of instrumenting the shock tube in various regions with pressure gauges and other diagnostics. The shock tube is placed on a mild steel stand and then placed on a 183-cm-tall

(6 ft) wooden stand to mitigate the influence of ground reflections at the shock tube exit (see Fig. 3). Overpressure data in all experiments are obtained using PCB Piezotronics 345-kPa (50-psi) blast pencil gauges placed either on the axis of the conical shock tube or 10 cm off-axis. The gauges are always placed either at the channel section exit (i.e., 216 cm from the nearest surface of the pentolite charge) or 30 cm downstream from the exit (246 cm from the charge surface).

Fig. 3 Explosively driven 10° conical shock tube, using an open-air test section, at one of the US Army Research Laboratory's outdoor experimental facilities; the blast gauges in the photograph are placed 30 cm downstream of the channel section exit

Four different test sections are investigated in the current work: 1) open air, 2) a cylinder, 3) a 10° square frustum that is inscribed by the circular cross section of the conical channel section exit, and 4) a 10° square frustum that is circumscribed by the channel section exit. Engineering sketches for the square frustum test sections are shown in Fig. 4. All test sections (other than the open air) are fabricated from 0.48-cm-thick mild steel and are 61 cm in length.

2.2 Shock Tube Metrics

In the ideal case where the boundary conditions provided by the shock tube walls perfectly mimic those seen by a spherical sector in a detonating sphere of energetic material, the shock tube cone angle and shock tube charge mass determine the mass associated with an equivalent spherical free-field charge (denoted as the effective free-field mass). The ratio of the effective free-field charge mass, m_{e}, to the mass

actually used in the shock tube, m_{s}, is termed the performance factor. The ideal performance factor, A_{i}, is determined from geometry and given as follows:

$$A_{\mathrm{i}}(\theta) = \frac{2}{1 - \cos\left(\frac{\theta}{2}\right)}, \tag{1}$$

where θ is the full angle of the spherical conic section as depicted in Fig. 1. Therefore, the ideal performance factor for the shock tube used in this work is simply

$$A_{\mathrm{i}}(10^{\circ}) \approx 525. \tag{2}$$

The actual shock tube performance factor, A_{a}, is always less than the ideal performance factor, A_{i}, and their ratio is termed the shock tube efficiency factor

$$\epsilon_{\mathrm{S}} = \frac{A_{\mathrm{a}}}{A_{\mathrm{i}}}. \tag{3}$$

The actual performance factor, A_{a}, is a property of both the shock tube angle and the driver section design and is defined as

$$A_{\mathrm{a}} = \frac{m_{\mathrm{e}}}{m_{\mathrm{s}}}. \tag{4}$$

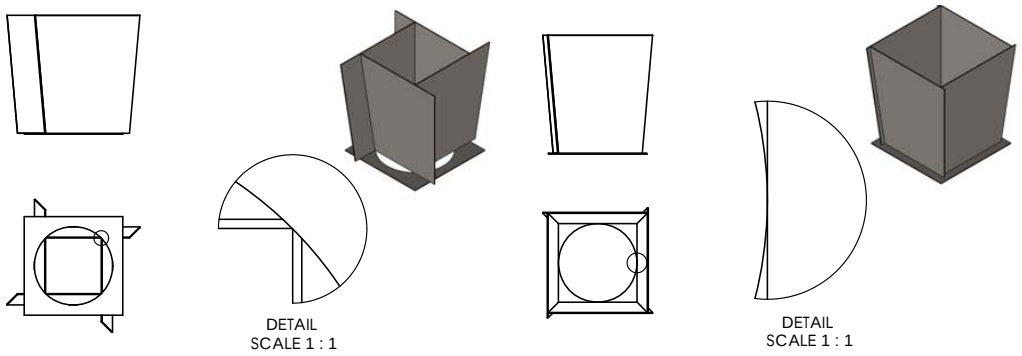

a) Circumscribed **b) Inscribed**

Fig. 4 Shock tube 10° square frustum test section geometries

2.3 Comparison with Free-Field Air Blast Estimates

Pressure-time histories due to explosively driven air blast have a distinct shape.[21] Friedlander[7] suggested an equation to describe the shock profile that agrees well with experimental data in the far-field. In the mid-field, where the peak overpressures are generally greater than 100 kPa but the air shock has already separated from the explosive product gases, Dewey[6] recommends the following modified form of the Friedlander equation:

$$P(t) = P_{\mathrm{S}} \mathrm{e}^{-\alpha t} \left(1 - \frac{t}{t^{+}}\right), \tag{5}$$

where $P(t)$ is the time-dependent overpressure, P_{S} is the peak overpressure, t is the time after the air blast arrival, t^{+} is the positive phase duration, and α is a shape factor. The original Friedlander equation may be recovered by setting $\alpha = 1/t^{+}$, resulting in the shape of the waveform being completely determined by the peak overpressure and positive phase duration.

Both the original and modified Friedlander waveforms are idealized representations of a free-field air blast environment, without any influence of shock reflections (from the ground, shock tube surfaces, etc.). Since the shock tube is a tool designed to approximate the free-field air blast, it is instructive to compare the shock tube data back to a Friedlander waveform. In this report, which focuses on the mid-field blast environment, shock tube experimental data is compared against the modified Friedlander waveform of Eq. 5.

The effective free-field mass, m_{e}, in Eq. 4 is estimated in this report using ConWep.[22] The estimation procedure is to identify 1) the peak incident overpressure from a single representative shock tube experiment (for the reference curves contained in this report, the peak overpressure measured at a gauge located both on the axis and at the interface between the channel and circumscribed test sections was used); and 2) the measurement location relative to the explosive charge in the experiment. ConWep is then used to determine the spherical free-field explosive charge mass (50/50 pentolite, in this case) that produces the same peak incident overpressure at the given standoff. The modified Friedlander equation can then be plotted by using the peak pressure, positive phase duration, and shape factor obtained from ConWep and adjusting the time of arrival to match the shock tube air blast time of arrival (typically the ConWep and shock tube times of arrival differ by

less than 5%). Table 1 gives the values of the parameters used to plot the modified Friedlander waveforms in this report, which correspond to an 816-g (1.8-lb) sphere of pentolite, at both 216 and 246 cm standoff.

Table 1 Modified Friedlander parameters, taken from ConWep, corresponding to an 816-g pentolite free-field charge

Distance from charge [cm]	P_S [kPa]	t^+ [ms]	α
216	163	2.01	1.176
246	123	2.33	0.973

3. Experimental Results

This section details experimental data obtained using 4 different test sections—1) open air, 2) cylindrical, 3) inscribed 10° square frustum, and 4) circumscribed 10° square frustum—attached to the end of a 10° conical shock tube driven by 5.3 g of pentolite. All shock tube data in this section are compared with modified Friedlander waveforms corresponding to an 816-g pentolite free-field charge, since this is the charge determined from ConWep to generate similar peak pressures as the shock tube at the measurement locations (216 and 246 cm from the charge surface, corresponding to the channel exit and approximately midway through the 61-cm-long steel test sections, respectively).

3.1 Open-Air Test Section

Figure 5 presents the incident overpressures and corresponding impulses obtained when an open-air test section is employed. This configuration is the most practical configuration when the use of optical diagnostics is required since there is nothing to block the view of the test item (e.g., no steel walls to look through). This test section configuration is the one used in Stewart and Pecora[18]—although with a different driver charge, driver section, and channel section than those used in the current work—and shows similar features to what was observed in that previous work.

The incident overpressures measured at the exit of the shock tube channel section (216 cm downstream) using the open-air test section (Fig. 5a) are seen to initially follow a modified Friedlander waveform before rapidly falling below ambient pressure due to the arrival of release waves. These release waves are generated from the

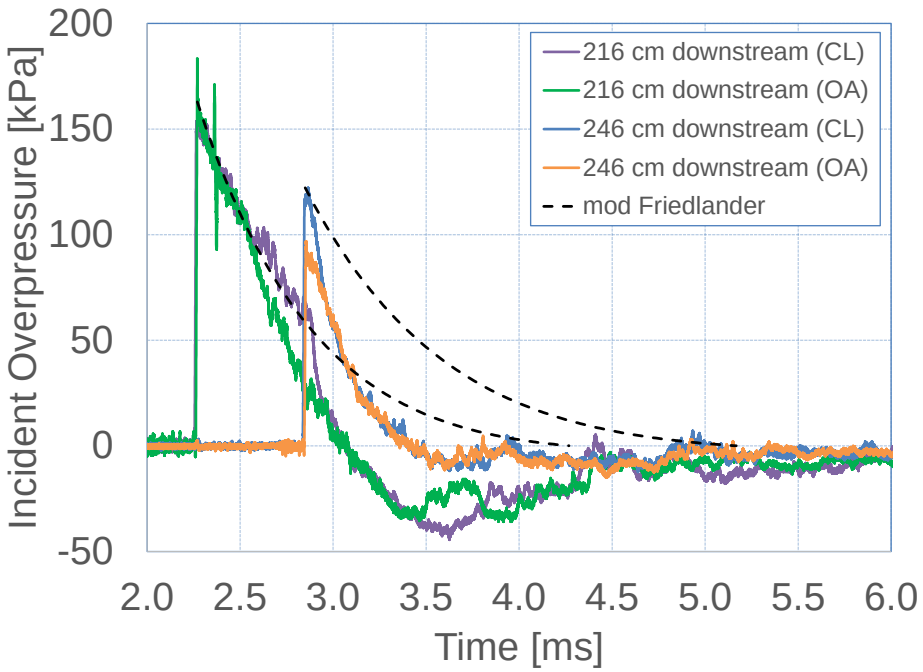

a) Incident Overpressures

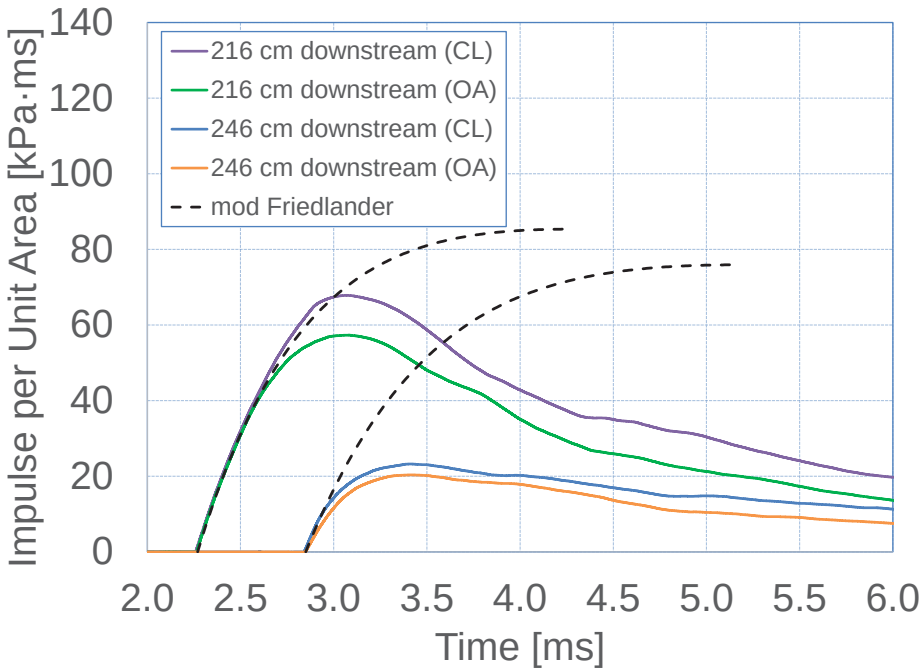

b) Impulse per Unit Area

Fig. 5 Open-air test section: shock tube experimental data taken both on the axis of symmetry (CL) and 10 cm off-axis (OA), along with modified Friedlander waveforms approximating an 816-g pentolite free-field charge

air blast exiting the confining steel tube that is the channel section and entering the surrounding ambient environment. The arrival of release waves is observed first on the off-axis data, as expected, since this gauge is closer to the end of the tube wall where the release waves are generated.

It is evident from comparing the Friedlander waveform with the incident overpressure data measured at 246 cm (i.e., 30 cm downstream of the channel section exit) that the arrival of the release waves have already degraded the peak pressure at the off-axis location and are just behind the arrival of the peak pressure on the axis. The influence of release waves 30 cm downstream of the channel exit is further demonstrated by comparing the peak overpressures with the modified Friedlander waveform at this location; the peak overpressure at the off-axis location is substantially lower than what would be expected from a free-field charge. Due to the influence of the release waves, the impulses measured using the open-air test section (Fig. 5b) never reach the peak impulses predicted from the modified Friedlander waveforms for a free-field blast environment—with the impulses measured 30 cm downstream of the channel section exit exhibiting particularly poor representations of the free-field environment.

3.2 Cylindrical Test Section

Figure 6 presents the incident overpressures and corresponding impulses obtained when a cylindrical test section is employed, as was presented in Stewart.[23] This test section configuration is not ideal for optical diagnostics since a conforming (i.e., curved) window presents challenges associated with refracting beams and since a flat window could disturb the flow coming through the tube. However, this geometry was considered because 1) it was not known beforehand whether planar test sections would be viable and 2) it was expected that the cylindrical geometry would be an improvement over simply extending the conical tube (e.g., windows are easier to manufacture for a cylinder than for a cone).

The peak incident overpressures measured at the channel section exit 216 cm downstream of the charge using a cylindrical test section (see Fig. 6a) are similar to those in the open-air configuration (as is expected since all experiments are nominally identical prior to reaching the test section) but there is no evidence of release waves with the cylindrical test section in place and the overpressures remain much closer to the modified Friedlander waveform throughout. Roughly $500\,\mu s$

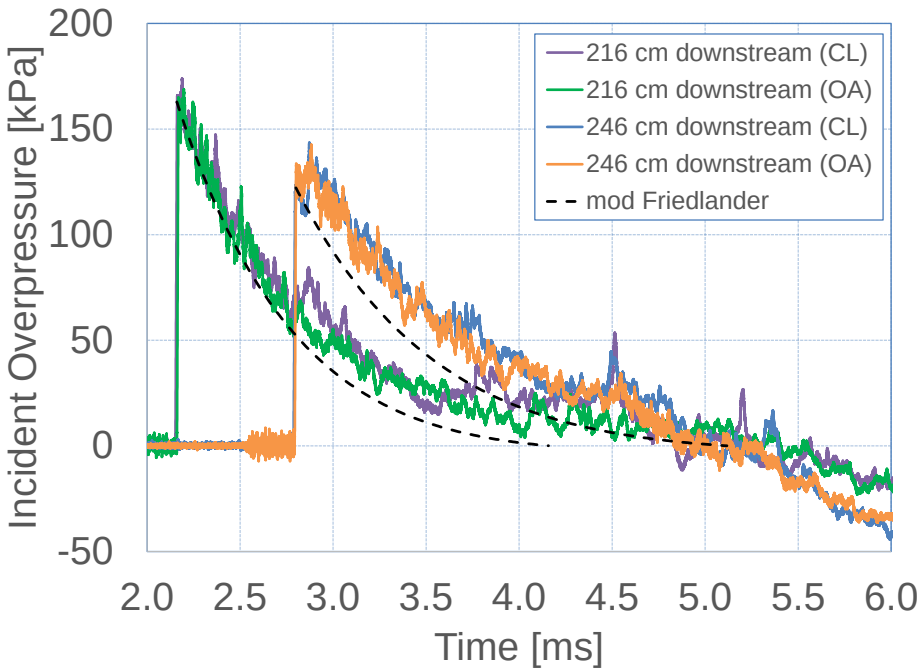

a) Incident Overpressures

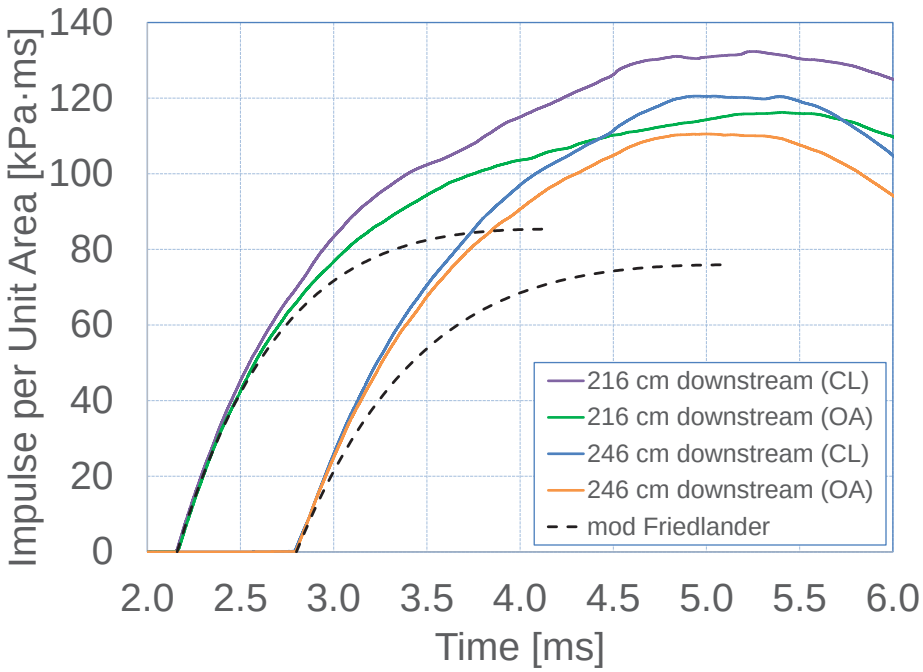

b) Impulse per Unit Area

Fig. 6 Cylindrical test section: shock tube experimental data taken both on the axis of symmetry (CL) and 10 cm off-axis (OA), along with modified Friedlander waveforms approximating an 816-g pentolite free-field charge

after the shock wave arrives at the channel section exit, as well as at the gauges located at the middle of the test section (i.e., 246 cm downstream of the charge), the measured overpressures are actually higher than the corresponding modified Friedlander waveforms; similar results are observed in the impulse data of Fig. 6b. These higher pressures and impulses relative to the free-field environment represented by the modified Friedlander waveforms are due to the constant cross-sectional area of the cylindrical test section. The conical channel section, similar to the free-field, allows the air blast to expand into an ever-increasing volume, which controls the shape of the waveform; however, once the flow enters the cylindrical test section, which is not a diverging geometry, the pressures are kept higher for longer, transmitting larger impulses.

3.3 Inscribed 10° Square Frustum Test Section

The third test section investigated is that of a 10° square frustum that is inscribed by the circular cross section of the conical channel section exit. The advantage of this geometry is that 1) a planar window can be easily installed to facilitate optical diagnostics and 2) the cross-sectional area of the inscribed square is larger than the cross-sectional area of the channel section, which makes it easier to place test items inside.

Figure 7 contains plots of the overpressures measured using the inscribed test section and the corresponding impulses along with the modified Friedlander waveforms approximating an 816-g pentolite free-field charge. At the channel section exit (216 cm downstream) there is indication prior to 3 ms of release waves generated by the flow exiting the channel section and expanding into the square frustum geometry of the test section (Fig. 7a). At the mid-point of the test section (246 cm downstream) there is evidence of a secondary shock, likely due to the air shock encountering the walls of the test section after the initial expansion. This secondary shock is especially evident from the gauge located on the axis at the mid-point of the test section. The release waves and secondary shock are less obvious in the impulse data plotted in Fig. 7b where the shock tube data provide a reasonable approximation of the free-field estimate denoted by the modified Friedlander waveforms.

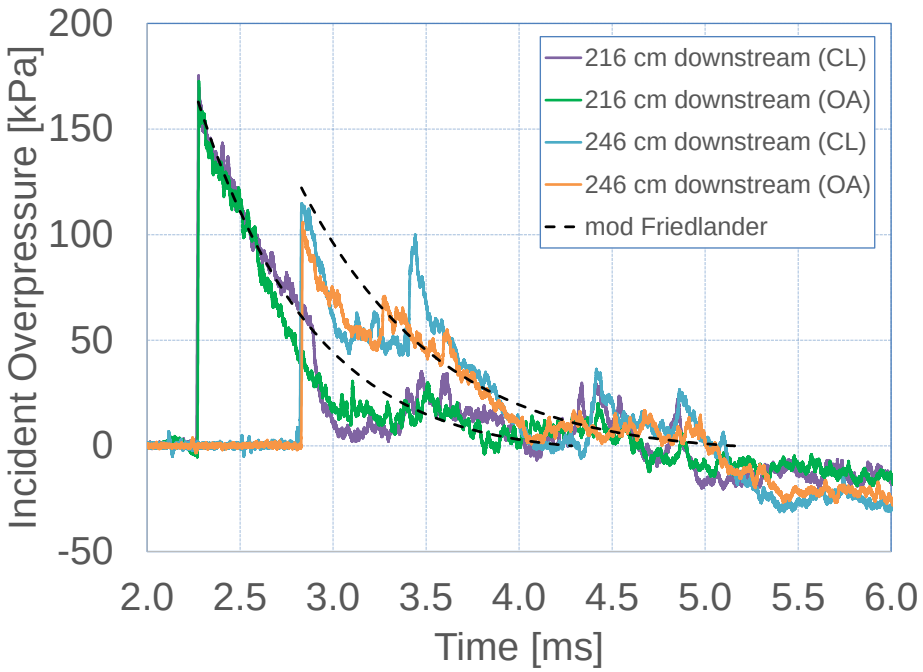

a) Incident Overpressures

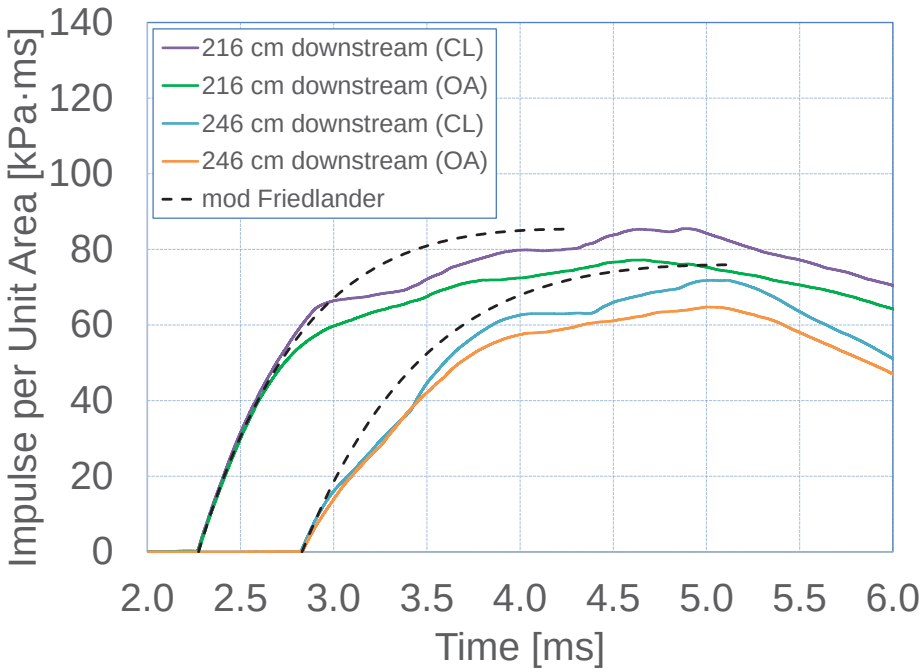

b) Impulse per Unit Area

Fig. 7 Inscribed 10° square frustum test section: shock tube experimental data taken both on the axis of symmetry (CL) and 10 cm off-axis (OA), along with modified Friedlander waveforms approximating an 816-g pentolite free-field charge

3.4 Circumscribed 10° Square Frustum Test Section

Lastly, a 10° square frustum circumscribed by the circular channel section exit, such that the flow coming out of the channel section is cut by square cross-section of the frustum, is used as the test section for the shock tube. The resulting incident overpressures and corresponding impulses are plotted in Fig. 8. This test section configuration would be ideal for optical diagnostics since a planar window could easily be installed. The main drawback of this configuration is that the cross-sectional area decreases relative to the circular cross-sectional area of the channel section, which could limit the size of test items that can be placed into the section.

Both the peak incident overpressures (Fig. 8a) measured using the blast gauges and the corresponding impulses (Fig. 8b) agree quite well with the modified Friedlander waveform approximating the free-field environment from a detonating 816-g pentolite sphere. Both the data at the channel section exit (216 cm downstream) as well as the data in the middle of the test section (246 cm downstream) show excellent agreement with the ConWep estimates (i.e., the modified Friedlander waveforms shown in the plots) of a free-field environment at the same respective location.

3.5 Discussion

Figures 5 through 8 presented data from a single experiment at each gauge location (i.e., the data at 216 cm were taken from a single experiment and the data taken at 246 cm were taken from a separate experiment). Each of these experiments was repeated, and the data from all experiments are tabulated in Table 2 along with the estimated effective free-field environment due to an 816-g pentolite sphere, which was obtained using ConWep. Table 2 lists for each experiment the air shock time of arrival, t_{a}; the maximum incident overpressure, $P_{\max}$, which is simply the maximum unfiltered pressure peak recorded from the pencil gauges; and the maximum impulse per unit area, $I_{\max}$. Data from 16 separate experiments are tabulated (gauges 1 and 2 were placed in 8 experiments and gauges 3 and 4 were placed in the other 8, so that the gauges and gauge stands would not interfere with each other). For example, in Table 2, row 1 of gauge 1 for a given configuration contains data from the same experiment as row 1 of gauge 2; likewise, row 2 of gauge 3 for a given configuration contains data from the same experiment as row 2 of gauge 4.

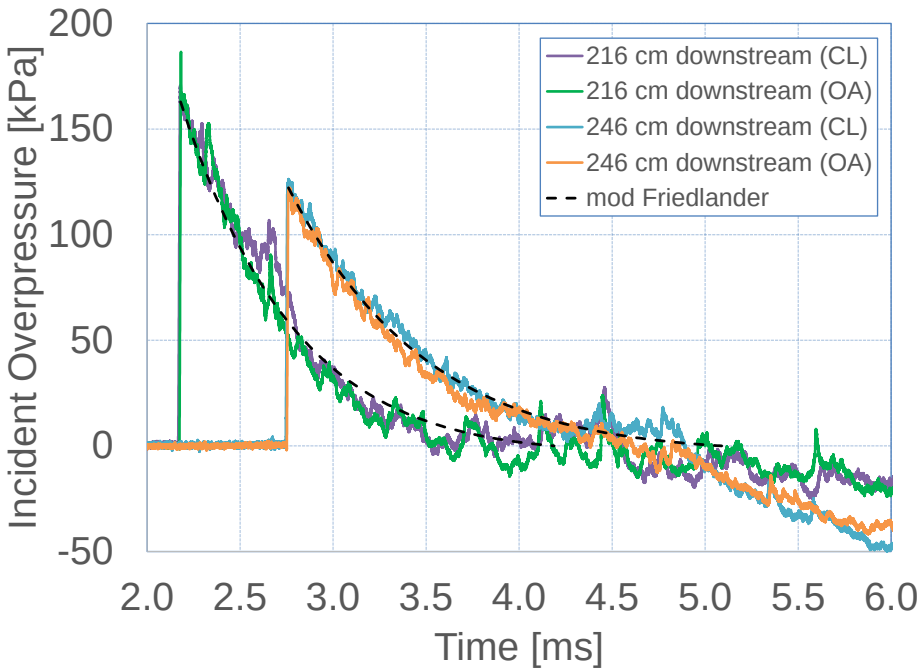

a) Incident Overpressures

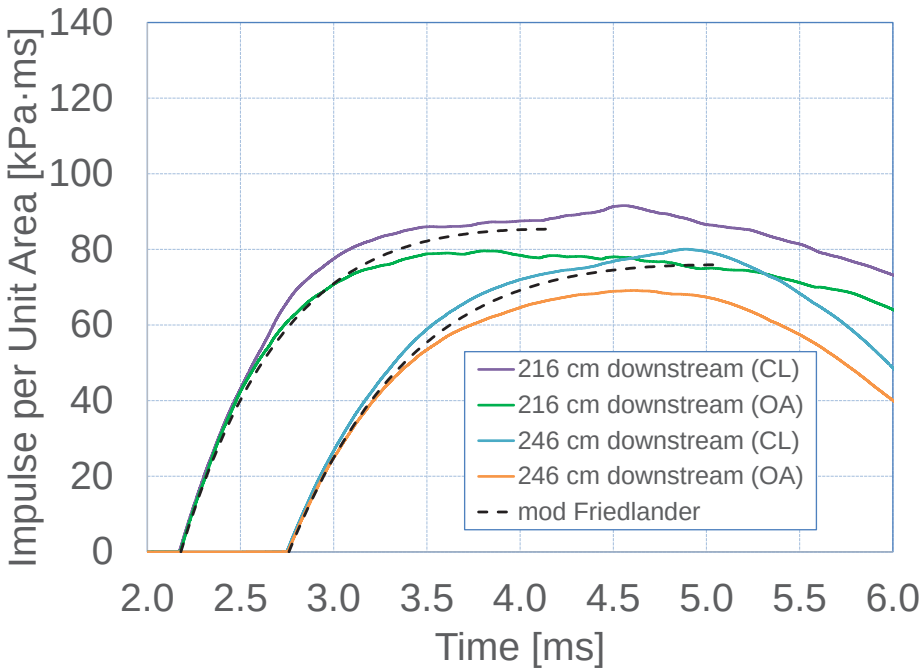

b) Impulse per Unit Area

Fig. 8 Circumscribed 10° square frustum test section: shock tube experimental data taken both on the axis of symmetry (CL) and 10 cm off-axis (OA), along with modified Friedlander waveforms approximating an 816-g pentolite free-field charge

Table 2 Shock tube air blast environment compared against ConWep free-field estimate

Configuration	Gauge[ab]	t_a [ms]	P_{max} [kPa]	I_{max} [kPa·ms]
Free-field estimate	1, 2	2.24	163	85.3
	3, 4	2.83	123	76.0
Open-air test section	1	2.27	155	67.8
		2.18	163	67.1
	2	2.27	184	57.3
		2.18	191	54.9
	3	2.85	122	23.2
		2.85	127	32.2
	4	2.86	96.9	20.3
		2.85	105	22.8
Cylindrical test section	1	2.16	174	132
		2.13	158	134
	2	2.17	169	116
		2.16	163	115
	3	2.80	144	121
		2.77	150	120
	4	2.80	143	111
		2.78	160	111
Inscribed 10° square frustum test section	1	2.27	163	88.3
		2.28	175	85.5
	2	2.28	172	80.0
		2.28	173	77.2
	3	2.79	116	75.6
		2.83	115	71.8
	4	2.75	77.6	64.4
		2.84	106	64.7
Circumscribed 10° square frustum test section	1	2.14	163	94.2
		2.18	171	91.6
	2	2.15	186	80.7
		2.18	187	79.6
	3	2.76	139	74.1
		2.76	126	80.0
	4	2.73	114	65.3
		2.76	122	69.1

[a] Gauges 1 and 2 are at the exit of the shock tube channel section, 216 cm downstream of the charge surface (gauges 1 and 2 are on-axis and 10 cm off-axis, respectively)

[b] Gauges 3 and 4 are 30 cm downstream of the shock tube channel section exit (on-axis and 10 cm off-axis, respectively)

Repeatability of the data tabulated in Table 2 seems reasonable and the shock tube data agree well with the free-field estimate using ConWep—especially for the circumscribed square configuration. The times of arrival of the air blast in the shock tube are all within 5% of the free-field estimate. The peak shock tube impulses calculated from the measured overpressures are always greater for a given experiment on the axis (gauges 1 and 3) than they are off-axis (gauges 2 and 4). This result could be due, in part, to wave curvature since the off-axis blast gauge is slightly further away radially from the explosive charge (taking either the detonator or the center of an effective spherical charge as the origin) relative to the centerline gauge.

Figure 9 presents the data from Table 2 graphically in terms of peak incident overpressure and peak impulse per unit area versus shock time of arrival. The purple symbols indicate data measured on the axis, while the green symbols denote off-axis data. ConWep free-field estimates corresponding to an 816-g pentolite free-field charge at the given standoff locations are shown as red diamonds.

Of the 4 test sections considered, the circumscribed 10° square frustum test section generated the best approximation of a free-field environment due to an 816-g sphere of pentolite (see Figs. 8 and 9 along with the data in Table 2). Figure 10 shows still frames taken from high-speed video looking down the test section of the shock tube toward the explosive charge during one of the experiments using the circumscribed 10° square frustum test section. Figure 10a shows the first frame for this particular experiment where detonation breakout is evident. Figure 10b shows a still frame from approximately 3 ms after detonation when the front of the air shock is inside the test section (not visible in the figure). Figure 10c shows a still frame from approximately 5 ms after detonation when the air shock has exited the test section. A fireball is evident toward the entry of the shock tube in this last frame due to explosive product gases escaping out of the back.

It is not evident in the frames shown in Fig. 10 but, depending on the natural lighting levels and on the position of the high-speed cameras, a vortex ring coming off the test section exit around 5 ms can be observed, similar to what was observed in Stewart and Pecora,[18] as well as debris burning both before and after impact with the steel pole holding the blast gauges. The type and source of this debris is not known but it could be still-reacting energetic material, detonator casing material, steel pieces from the sacrificial driver section, or something else not yet considered.

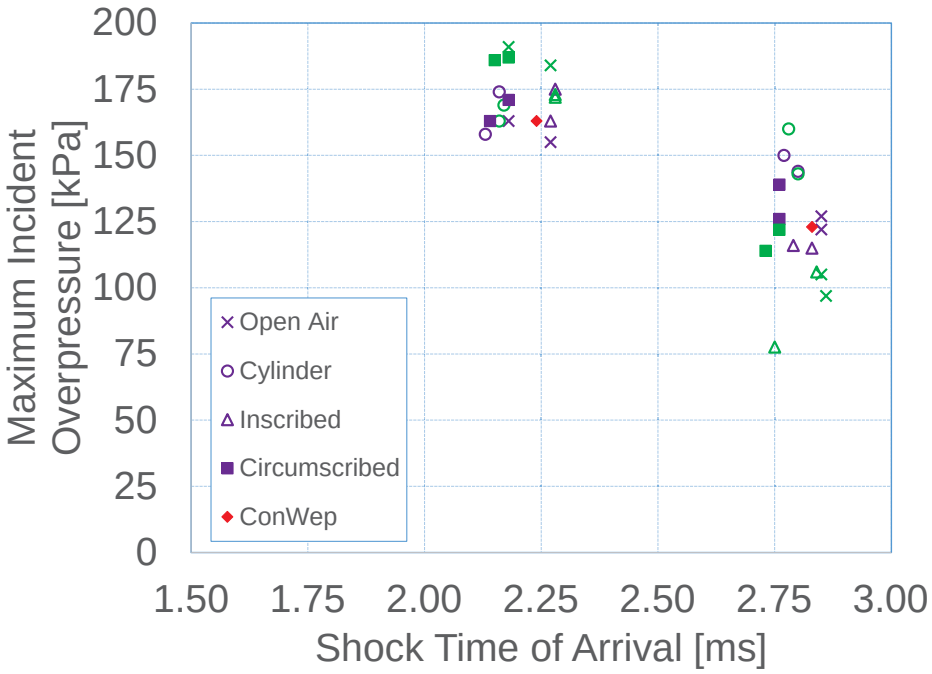

a) Incident Overpressures

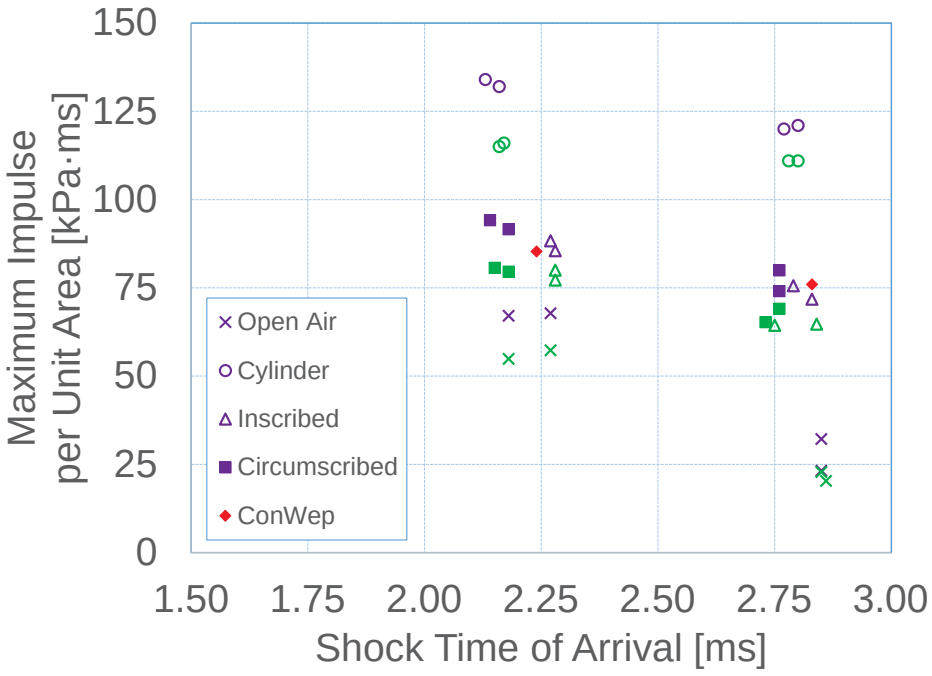

b) Impulse per Unit Area

Fig. 9 Experimental data from all shock tube test sections, both at the channel section exit and 30 cm downstream, along with ConWep free-field estimates. Purple symbols indicate data measured on the axis, while green symbols denote off-axis data.

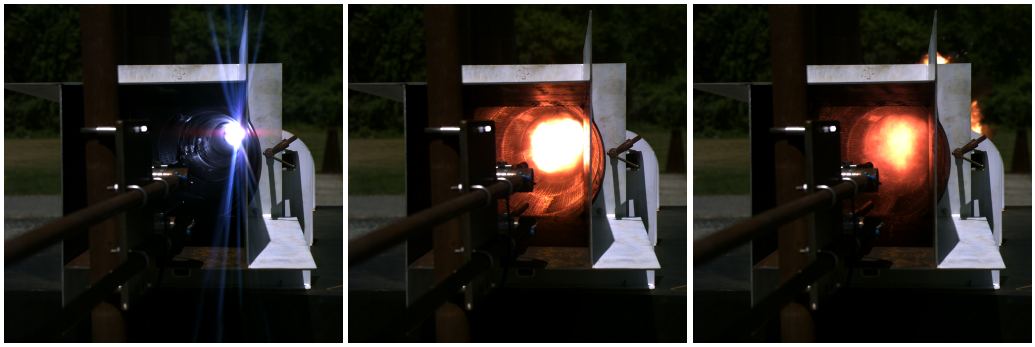

a) t=0 **b) t≈3 ms** **c) t≈5 ms**

Fig. 10 High-speed video still frames taken from a shock tube experiment using a circumscribed square frustum: times correspond to a) detonation breakout, b) air shock inside test section, and c) air shock outside of the test section

In the current work using a 10° shock tube and a 5.3-g pentolite charge with an open driver section, the pressure peak and initial decay of the air blast correspond to a modified Friedlander waveform of an 816-g sphere of pentolite for all test sections considered. This results in the following values for the actual performance factor and corresponding efficiency factor, using (2)–(4) along with m_{s} =5.3 g and m_{e} =816 g:

$$A_{\mathrm{a}} \approx 155, \tag{6}$$

and

$$\epsilon_{\mathrm{S}} \approx 30\%. \tag{7}$$

For comparison, the previous shock tube work documented in Stewart and Pecora[18] using a 17° shock tube and 14.5-g C4 charge can be fit to a modified Friedlander waveform corresponding to an 862-g sphere of C4. These previous results translate to a performance factor of roughly 60 and efficiency factor of 33%. The similar efficiency factors of roughly 30% obtained in both the current and previous explosively driven shock tube experimental series likely point to the similar open-back driver housing sections used in both experimental series (in contrast, Stewart[23] demonstrated efficiencies of roughly 50–70% using the 10° channel section with a closed-back driver housing section).

4. Summary and Conclusion

An explosively driven 10° conical shock tube with a 5.3-g pentolite shock tube driver charge and an open-back driver housing section was used to produce the peak overpressures corresponding to a free-field detonation from an 816-g sphere of pentolite. Four test sections were evaluated for use with the shock tube:

- The open-air test section performed similarly to previous work and showed a pronounced effect from release waves generated by the open exit of the channel section. These release waves resulted in much lower impulses than would be expected from the equivalent 816-g pentolite sphere free-field detonation.
- Due to its non-diverging geometry, the cylindrical test section resulted in higher overpressures and impulses relative to what would be expected from the equivalent free-field detonation.
- The inscribed 10° square frustum test section resulted in both release waves and a secondary shock but provided adequate agreement with the free-field estimates in terms of the impulse time histories.
- The circumscribed 10° square frustum test section resulted in good agreement with the free-field estimates of both incident overpressure and impulse time histories.

Future work will focus on installing a window into the circumscribed 10° square frustum test section and using optical diagnostics to better study the blast environment.

5. References

1. Davy H. On the fire-damp of coal mines, and on methods of lighting the mines so as to prevent its explosion. Philosophical Transactions of the Royal Society of London. 1816;106:1–22.

2. Dixon HB. On the movements of the flame in the explosion of gases. Philosophical Transactions of the Royal Society of London, Series A, Containing Papers of a Mathematical or Physical Character. 1903;200:315–352.

3. Bleakney W, Weimer DK, Fletcher CH. The shock tube: a facility for investigations in fluid dynamics. Review of Scientific Instruments. 1949;20(11):807–815.

4. Ritzel D, Matthews K. An adjustable explosion-source model for CFD blast calculations. In: Proceedings of 21st International Symposium on Shock Waves; 1997 Jul; Great Kevvel Island, Australia. p. 97–102.

5. Ritzel DV, Parks SA, Roseveare J, Rude G, Sawyer TW. Experimental blast simulation for injury studies. In: Proc. HFM-207 NATO Symposium on a Survey of Blast Injury Across the Full Landscape of Military Science; 2011 Oct; Halifax, Nova Scotia, Canada. p. 11-1 – 11-20.

6. Dewey JM. The shape of the blast wave: Studies of the Friedlander equation. In: Proceedings of the 21st International Symposium on Military Aspects of Blast and Shock; p. 22–30.

7. Friedlander FG. The diffraction of sound pulses. i. diffraction by a semi-infinite plane. Proceedings of the Royal Society of London A: Mathematical, Physical and Engineering Sciences. 1946;186(1006):322–344.

8. Stewart J. Approximating a free-field blast environment in the test section of an explosively driven conical shock tube. Shock Waves; 2018 Feb https://doi.org/10.1007/s00193-018-0811-7.

9. Elsayed NM. Toxicology of blast overpressure. Toxicology. 1997;121(1):1–15.

10. Reneer DV, Hisel RD, Hoffman JM, Kryscio RJ, Lusk BT, Geddes JW. A multi-mode shock tube for investigation of blast-induced traumatic brain injury. Journal of Neurotrauma. 2011;28(1):95–104.

11. Shridharani J, Wood GW, Panzer MB, Capehart BP, Nyein M, Radovitzky RA, Bass CR. Porcine head response to blast. Frontiers in Neurology. 2012;3:70.

12. Sundaramurthy A, Alai A, Ganpule S, Holmberg A, Plougonven E, Chandra N. Blast-induced biomechanical loading of the rat: an experimental and anatomically accurate computational blast injury model. Journal of Neurotrauma. 2012;29(13):2352–2364.

13. Courtney AC, Andrusiv LP, Courtney MW. Oxy-acetylene driven laboratory scale shock tubes for studying blast wave effects. Review of Scientific Instruments. 2012;83(4):045111-1 – 045111-7.

14. Courtney E, Courtney A, Courtney M. Shock tube design for high intensity blast waves for laboratory testing of armor and combat material. Defense Technology. 2014;10:245–250.

15. Filler WS. Measurements of the blast wave in a conical tube. The Physics of Fluids. 1960;3(3):444–448.

16. Filler WS. Propagation of shock waves in a hydrodynamic conical shock tube. The Physics of Fluids. 1964;7(5):664–667.

17. Zalesak JF, Poché, Jr. LB. The shock test facility: An explosive-driven, water-filled conical shock tube. In: 60th Shock and Vibration Symposium; Vol. III; 1989 Nov; Virgina Beach, VA. p. 73–76.

18. Stewart JB, Pecora C. Explosively driven air blast in a conical shock tube. Review of Scientific Instruments. 2015;86(3):035108.

19. McNesby KL, Homan BE, Benjamin RA, Boyle VM, Densmore JM, Biss MM. Quantitative imaging of explosions with high-speed cameras. Review of Scientific Instruments. 2016;87(5):051301.

20. Stewart JB. Considerations for explosively driven conical shock tube design: Computations and experiments. Aberdeen Proving Ground (MD): Army Research Laboratory (US); 2017 Feb. Report No.: ARL-TR-7953.

21. Kinney GF, Graham KJ. Explosive shocks in air. New York (NY): Springer Science and Business Media; 1985.

22. Hyde DW. Microcomputer programs CONWEP and FUNPRO, applications of TM 5-855-1, fundamentals of protective design for conventional weapons (user's guide). Vicksburg (MS): Army Corps of Engineer Waterways Experiment Station Structures Lab; 1988. Report No.: WES/IR/SL-88-1.

23. Stewart JB. Influence of explosively driven shock tube configuration on the mid field blast environment. In: Proceedings of the 20th Biennial APS Conference on Shock Compression of Condensed Matter; 2017 July; St Louis, MO.

INTENTIONALLY LEFT BLANK.

1 (PDF) DEFENSE TECHNICAL INFORMATION CTR DTIC OCA

2 (PDF) DIR ARL
IMAL HRA
RECORDS MGMT
RDRL DCL
TECH LIB

1 (PDF) GOVT PRINTG OFC
A MALHOTRA

1 (PDF) AFRL
R DORGAN

1 (PDF) AFOSR
M SCHMIDT

2 (PDF) LANL
L HILL
P BOWDEN

2 (PDF) DSTL (UK)
A SEDMAN
J WEIR

40 (PDF) DIR USARL
RDRL WMP
D LYON
RDRL WMP A
S BILYK
RDRL WMP B
C HOPPEL
A DILEONARDI
K RAFAELS
T WEERASOORIYA
RDRL WMP C
S SATAPATHY
R BECKER
RDRL WMP D
J RUNYEON
R DONEY
S SCHRAML
RDRL WMP E
P SWOBODA
RDRL WMP F
N GNIAZDOWSKI
C CUMMINS
E FIORAVANTE
RDRL WMP G
B ROOS
J ANDERSON
J BOYD
V BOYLE
P DUVALL
R FRANCART
B HOMAN
D KOOKER
S KUKUCK
C PECORA
J PIERCE
J RACINE
R SPINK
J STARKENBERG
L STEVENSON
J STEWART
RDRL WML C
D MEGONNELL
K MCNESBY
T PIEHLER
G SUTHERLAND
RDRL WMC
D HASH
G CHANEY
B HALL
J GYOLAI
D WEYAND

INTENTIONALLY LEFT BLANK.